REPORT DOCUMENTATION PAGE

Form Approved
OMB No. 0704-01-0188

PLEASE DO NOT RETURN YOUR FORM TO THE ABOVE ADDRESS.

1. REPORT DATE *(DD-MM-YYYY)*	2. REPORT TYPE	3. DATES COVERED *(From - To)*
21-06-2007	REPRINT	

4. TITLE AND SUBTITLE

Nascap-2k Self-Consistent Simulations of a VLF Plasma Antenna

5a. CONTRACT NUMBER

5b. GRANT NUMBER

5c. PROGRAM ELEMENT NUMBER
61102F

6. AUTHORS
M.J. Mandell*, V.A. Davis*, D.L. Cooke, A.T. Wheelock, and C.J. Roth**

5d. PROJECT NUMBER
1010

5e. TASK NUMBER
RR

5f. WORK UNIT NUMBER
A1

7. PERFORMING ORGANIZATION NAME(S) AND ADDRESS(ES)

Air Force Research Laboratory /VSBXT
29 Randolph Road
Hanscom AFB, MA 01731-3010

8. PERFORMING ORGANIZATION REPORT NUMBER
AFRL-VS-HA-TR-2007-1091

9. SPONSORING/MONITORING AGENCY NAME(S) AND ADDRESS(ES)

10. SPONSOR/MONITOR'S ACRONYM(S)
AFRL/VSBXT

11. SPONSOR/MONITOR'S REPORT NUMBER(S)

12. DISTRIBUTION/AVAILABILITY STATEMENT
Approved for Public Release; distribution unlimited.

13. SUPPLEMENTARY NOTES
Reprinted from Proceedings, 10th Spacecraft Charging Technology Conference, 18-21 June 2007, Biarritz, France .
* Science Applications International Corp., San Diego, CA 92121 * *Atmospheric and Environmental Research, Inc., Lexington, MA 02421

14. ABSTRACT

We simulate the plasma response to a high voltage square wave VLF antenna in Medium Earth Orbit plasma with *Nascap-2k*. The plasma is modeled with a hybrid Particle-in-cell (PIC) approach with PIC ions and fluid barometric electron densities. The plasma response, collected ion currents, and chassis floating potential are computed self-consistently with a near-square-wave bias applied to the antennas. Particle injection and splitting are used to replenish the plasma depleted at the boundary, represent the thermal distribution, and maintain appropriately sized macroparticles. Therefore, current limitation due to the thermal distribution of ions and the resulting angular momentum barrier are included. Above the ion plasma frequency the plasma current lags the voltage by about 10°, while below the ion plasma frequency the current leads the voltage by about 7°.

15. SUBJECT TERMS
VLF Plasma Simulation, Nascap-2k

16. SECURITY CLASSIFICATION OF:			17. LIMITATION OF ABSTRACT	18. NUMBER OF PAGES	19a. NAME OF RESPONSIBLE PERSON
a. REPORT	b. ABSTRACT	c. THIS PAGE			Adrian Wheelock
UNCL	UNCL	UNCL			19B. TELEPHONE NUMBER *(Include area code)*

NASCAP-2K SELF-CONSISTENT SIMULATIONS OF A VLF PLASMA ANTENNA

M. J. MANDELL and V.A. DAVIS

Science Applications International Corporation

10260 Campus Point Dr., M.S. A1A, San Diego, CA, 92121

D. L. COOKE and A.T. WHEELOCK

Space Vehicles Directorate

Air Force Research Laboratory/VSBX

Hanscom AFB, MA, 01731-3010

C. J. ROTH

Atmospheric and Environmental Research Inc.

131 Hartwell Ave., Lexington MA, 02421-3126

ABSTRACT: *We simulate the plasma response to high voltage square wave VLF antenna in Medium Earth Orbit plasma with Nascap-2k. The plasma is modeled with a hybrid Particle-in-cell (PIC) approach with PIC ions and fluid barometric electron densities. The plasma response, collected ion currents, and chassis floating potential are computed self-consistently with a near-square-wave bias applied to the antennas. Particle injection and splitting are used to replenish the plasma depleted at the boundary, represent the thermal distribution, and maintain appropriately sized macroparticles. Therefore, current limitation due to the thermal distribution of ions and the resulting angular momentum barrier are included. Above the ion plasma frequency the plasma current lags the voltage by about 10°, while below the ion plasma frequency the current leads the voltage by about 7°.*

1 - INTRODUCTION

The response of a plasma to very low frequency (VLF) (3 kHz to 20 kHz) high-voltage antennas at orbital altitudes of 1000 to 10,000 kilometers has been a subject of scientific interest for many decades.[1,2,3] Plasma waves from VLF antennas with such frequencies ("whistler" waves) are thought to interact with MeV radiation belt electrons. As this antenna frequency is less than both the electron plasma frequency and the electron gyrofrequency (both nearly 300 kHz for a plasma density of 10^9 m^{-3} and a magnetic field of 0.1 gauss), only certain modes can propagate as electromagnetic waves, and the near field is dominated by electrostatic effects. Although a comprehensive self-consistent electromagnetic-electrostatic simulation would be the desired goal, there are many computational challenges to be overcome, so we begin with electrostatic simulations in order to sort out the dominant plasmadynamic effects.

A VLF dipole antenna has two elements, each several centimeters in diameter and many meters long. Due to the ease of electron collection by positive objects, the positive element is at near zero or small positive potential relative to the ambient ionosphere, while nearly the full applied potential appears on the negative element. Because the frequencies of interest are comparable to the ion plasma frequency, the sheath structure is at some intermediate state between the "ion matrix" or "frozen ion" limit (which assumes the ions are stationary and contribute ambient ion density to the space charge) and the equilibrium space charge limit (in which the ions assume a steady-state space charge limited distribution of charge and current). Thus, calculation of the sheath structure and of the ion collection by the antenna requires dynamic (specifically, particle-in-cell, PIC) treatment, at least for the ions. *Nascap-2k* can be used to perform all four simulations of interest: (1) equilibrium space charge sheath; (2) "frozen ion" sheath; (3) dynamic PIC ions with fluid (Boltzmann or barometric) electrons (Hybrid PIC); (4) dynamic PIC ions and electrons (Full PIC). Previously we reported on one and three dimensional Full PIC calculations[4] and Hybrid PIC calculations with prescribed potentials for a higher density plasma.[5]

This paper presents antenna simulations performed with *Nascap-2k*. The plasma is modeled using the hybrid PIC approach with PIC ions and fluid barometric electron densities. The plasma response, collected ion currents, and chassis floating potential are computed self-consistently with a near-square-wave bias applied to the antennas. Current limitation due to the thermal distribution of ions and the resulting angular momentum barrier are included. The different plasma response above and below the ion plasma frequency are shown.

In order to perform these calculations, *Nascap-2k*'s PIC capability has been expanded to include boundary injection and particle splitting. The boundary injection replaces particles that are either collected or leave the problem in long-running calculations. The particle splitting allows for modeling of the effects of the thermal distribution of velocities, as well as reducing particle size when passing into regions of finer resolution. The algorithms used for these capabilities along with their accuracy and limitations are discussed.

2 - PARTICLE IN CELL TECHNIQUES

Nascap-2k has primarily been used to model quasi-static phenomena. However, there are a large number of physical processes of interest whose timescales require a dynamic approach such as a particle-in-cell (PIC) technique. Examples of such processes are breakdown phenomena, plasma kinetics, and sheath structure about surfaces with potentials that change on a timescale comparable to the time it takes an ion to cross the sheath. PIC techniques can also be used to address problems in which analytic representations of the environmental currents are inadequate, such as in a spacecraft wake or in a cavity. A steady-state PIC technique, in which the ion space charge density is computed from macroparticles tracked from the boundary of the computational space until they are collected or exit the computation space, was successfully used to model the CHAWS experiment.[6] In addition, PIC techniques can be useful when developing analytic models. In order to facilitate these modeling techniques, the ability to perform various types of PIC calculations was built into *Nascap-2k*. Recently, additional numeric techniques have been added to make two types of PIC calculations more flexible, robust, and faster—Hybrid PIC and Full PIC. In a Hybrid PIC calculation, the problem is initialized by creating ion macroparticles throughout the grid to represent a constant particle density. The ion macroparticles are tracked for one timestep and then volume potentials are computed using the resulting ion density and a barometric electron density.

$$\frac{\rho}{\varepsilon_o} = \frac{\rho_i}{\varepsilon_o} + \begin{cases} -(\phi+\theta)/\lambda^2 & \text{for } \phi > 0 \\ -\left(\theta/\lambda^2\right)\exp(\phi/\theta) & \text{for } \phi \le 0 \end{cases}$$

where ϕ and θ are the plasma potential and temperature and λ is the debye length. The process is repeated for the time period of interest. In a Full PIC calculation both electron and ion macroparticles are tracked and volume potentials are computed using the resulting plasma density.

Two recent enhancements to *Nascap-2k*'s PIC capabilities are the injection of macroparticles from the boundary during a calculation and the splitting of the macroparticles.

In order to replace macroparticles that are collected by the probe or escape from the grid, it is necessary to periodically inject macroparticles from the boundary. This allows for the calculation of current for longer time periods. In hybrid PIC calculations without boundary injection, the low field region near the boundary of the problem develops a significant negative potential due to ion depletion. Boundary injection keeps these potentials near zero by replenishing the ions that have been collected or escaped.

Particle injection is implemented with an injection point at each quarter-boundary-surface-element. The injected particle has charge equal to the plasma thermal current times the area times the time interval and velocity equal to $\sqrt{\frac{2eT}{\pi m}}$, so that it represents the inbound half of the plasma density. When the spacecraft is moving through the plasma this algorithm is modified to account for the motion. The current and velocity are computed in such a way that the density contribution of the injected particles varies from half the ion density for a stationary object to the full ion density for a high Mach number object.

Closely connected with boundary injection is macroparticle splitting. There are two major reasons for splitting macroparticles: one physical and one numeric. Even at moderate potentials, thermal effects can reduce collected currents. Some particles near the sheath edge have enough thermal velocity perpendicular to the electric field that angular momentum conservation prohibits collection. Particle splitting allows for a representation of the thermal distribution in the initial particle distribution and in particles injected from the boundary. From a numeric point of view, particle splitting can be used to keep the particle weight appropriate to the grid size and to help maintain the smoothness of the distribution. A large particle that originated in an outer grid is split in velocity in such a way that it preserves the plasma temperature and eventually becomes distributed over several volume elements in an inner grid.

Macroparticles may be split when they enter a more finely resolved region or when they are created either at the boundary or throughout the volume at problem initialization. The algorithm used is as follows:

1. Particles are split in velocity space only. Because high-field regions are often of interest, spatial splitting would raise problems with energy conservation.
2. Each particle carries a temperature, which is treated as isotropic. The fission products carry half the temperature of the original particle, while the remaining thermal energy appears as kinetic energy of the split particles. That each macroparticle has a temperature means that they can be split repeatedly, each time the particle enters a more finely resolved region.
3. For splitting purposes the Z-axis is defined to be along the direction of the particle velocity, the X-axis randomly chosen in the plane normal to Z, and the Y-axis mutually perpendicular.
4. Particles are split into two or three particles along each axis, except that a particle is not split along the Z-direction if the kinetic energy exceeds the thermal energy. Not splitting along Z helps avoid particle proliferation, but makes a small error by not preserving the original particle temperature along Z. Eight, nine, or twenty-seven new particles result.
5. Particle velocity is assumed to be acquired by acceleration rather than actual drift (i.e., spacecraft velocity). If there is actual drift, then the drift velocity is removed before splitting the particle and added back after.

6. If the particle is split by two along the X or Y axis, the new velocities are $\pm 0.707\sqrt{T/m}$. Along the Z axis the velocity increment is calculated as if the temperature were $T - 2mu_0^2\left(\sqrt{1+\frac{T}{mu_0^2}}-1\right)$.

7. If the particle is split by three along the X or Y axis, there is a zero-velocity central particle and two "probe" particles with velocity $\pm 0.866\sqrt{T/m}$. Along the Z axis the velocity increment is calculated as if the temperature were $T - 2mu_0^2\left(\sqrt{1+\frac{T}{mu_0^2}}-1\right)$.

The new particles have the same properties as the original particle except for velocity, weight (charge), and temperature.

3 - SELF-CONSISTENT ANTENNA CALCULATIONS

We performed a series of calculations of three-dimensional, time-dependent, self-consistent potentials and currents for a spacecraft with a VLF transmitting antenna. The *Nascap-2k* model used is shown in Figure 1 and **Figure 2**. The body is a 1.6 m aluminum cube and the two six-sided antennas are 0.05 m in diameter and 25 m long (3.75 m^2 each). The grid used for the calculations is shown in Figure 3 and Figure 4. The mesh unit of the outermost grid is 2 m.

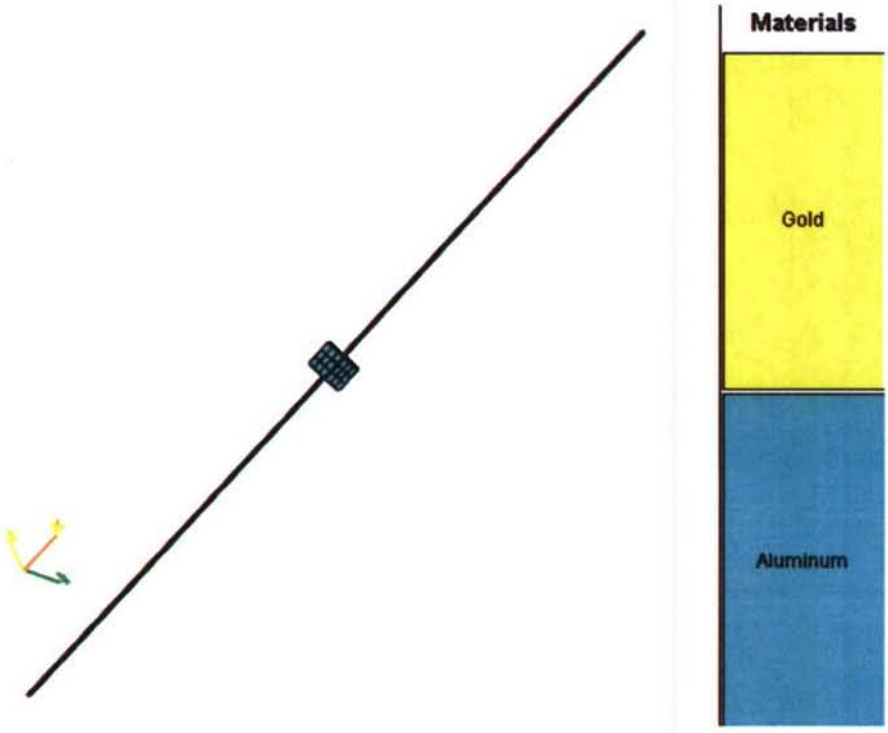

Figure 1. *Nascap-2k* model of VLF transmitting spacecraft.

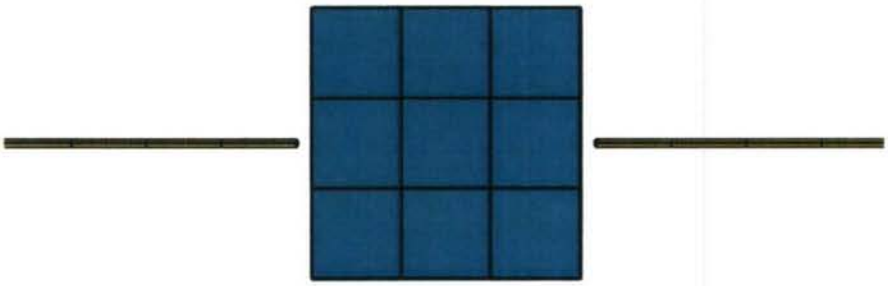

Figure 2. Expanded view of center portion of *Nascap-2k* model of VLF transmitting spacecraft.

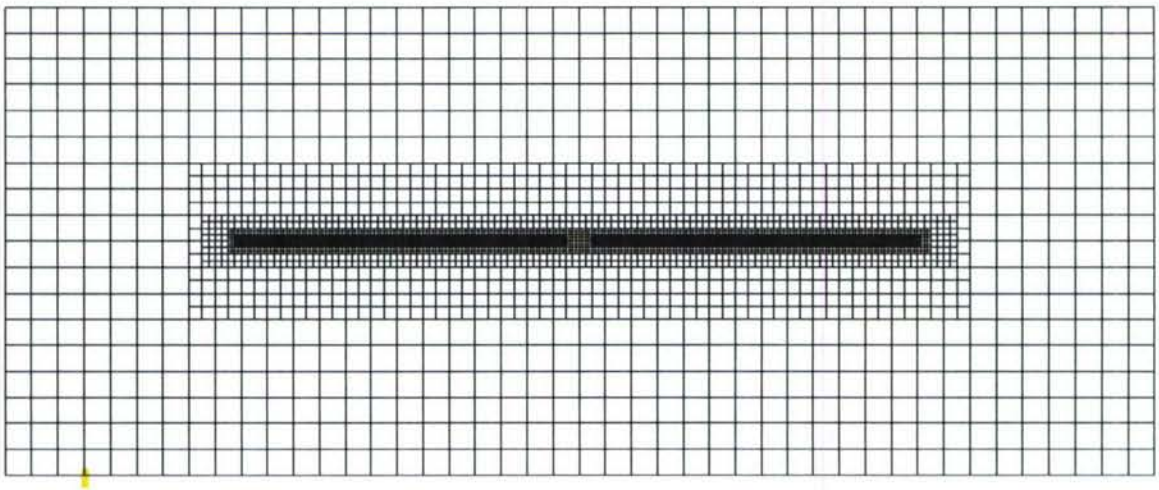

Figure 3. Grid used for VLF antenna calculations.

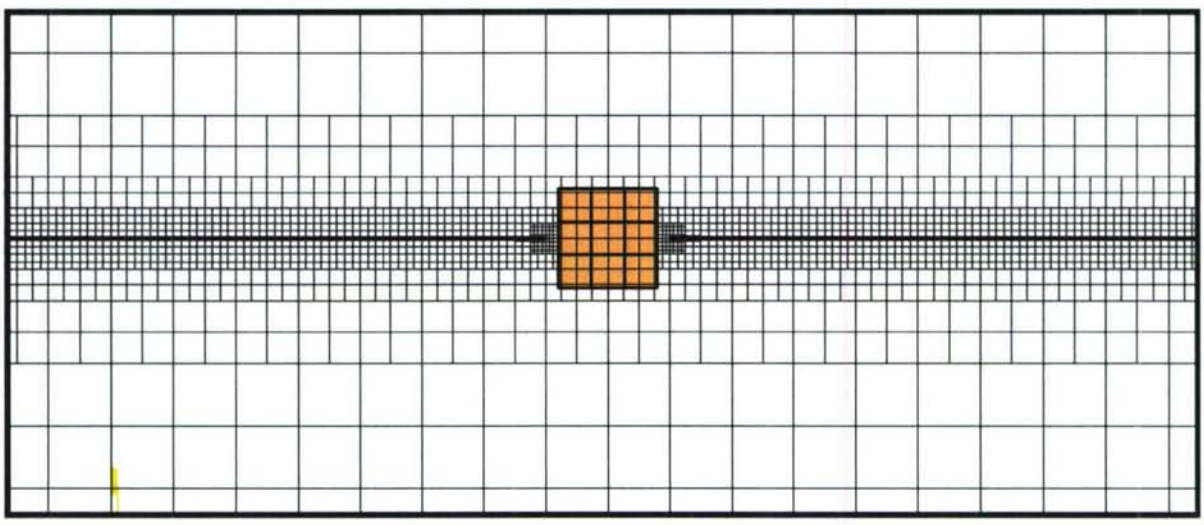

Figure 4. Close-up of center of grid used for antenna calculations.

Results from four calculations are shown below. The parameters of the calculations are shown in Table 1. In all cases, the potentials are adjusted to account for the incident current each timestep. The incident current is the tracked ion current together with an analytic electron current given by

$$I = \begin{cases} A j_{th} \exp(\phi/\theta) & \text{if } \phi \le 0 \\ A j_{th}\left(1+\dfrac{\phi}{\theta}\right) & \text{if } \phi > 0 \end{cases}$$

where A is the surface area and j_{th} is the plasma thermal current. One antenna is floating and the other has a variable bias with respect to the first. The aluminum box is floating. The timestep is set so that macroparticles move a reasonable distance each timestep. The Hybrid PIC charge density model is used.

The bias applied between the antenna elements is the sum of four Fourier components that approximates a square wave with amplitude of 1 kV and the indicated frequency, as shown in Figure 5. In the absence of plasma, each antenna element switches between ±500 V. The square wave excitation is desirable in order to minimize time spent at low potentials, for which the plasma capacitance is highly variable. Having a phase-independent capacitance makes it easier to tune the power supply for optimal operation.

Table 1. Parameters used in antenna calculations.

	Case 1	Case 2	Case 3	Case 4
Density (m^{-3})	10^8	10^8	10^9	10^9
Temperature (eV)	1	1	1	1
Species	H^+	H^+	H^+	H^+
Ion plasma frequency (kHz)	2	2	6.6	6.6
Frequency (kHz)	10	10	12	2
Splitting of initial macroparticles	None	All grids	All grids	All grids
Splitting on subgrid entry	None	Three levels	Three levels	Three levels
Macroparticle injection	None	Every 14 timesteps	Every 10 timesteps	Every timestep
Number of macroparticles (millions)	0.50	3.9 to 13.1	3.9 to10.4	2.9 to 12.2
Current (mA)	0.2	0.03	0.3	0.25
Phase shift	~0°	10°	12°	-7°

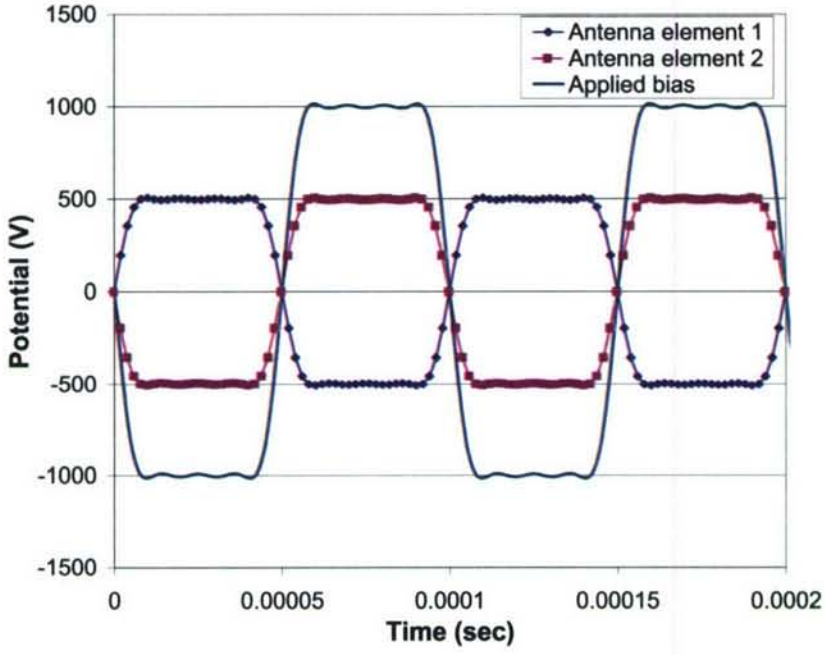

Figure 5. Applied bias values and resulting antenna potentials in the absence of a plasma.

The first two calculations are for tenuous plasma (10^8 m^{-3}) with excitation frequency well above the ion plasma frequency. Figure 6 shows the potential of the antenna elements and spacecraft body for Case 1, which has no particle splitting. In the initial few cycles the positive antenna element collects substantial electron current, driving the mean antenna potential to about -500 V. The spacecraft body initially follows this transient due to capacitive coupling, reaching negative potential of nearly 200 V, from which it gradually recovers. During the switching time from one polarity to the other there is a period during which both antenna elements are negative, and thus collecting some ions but no electrons. This causes the positive element to spike at positive potential following the switch, and the positive potential gradually decays during the half cycle.

Figure 7 shows the average surface current to an antenna element for the case with no particle splitting. As expected, the current is very noisy due to lack of splitting. It is also, at 0.2 mA (50 $\mu A\ m^{-2}$), much larger than the 2 $\mu A\ m^{-2}$ orbit limited current for a cylinder accounting for the thermal angular momentum. This is as expected, since without splitting the thermal velocity distribution is not represented.

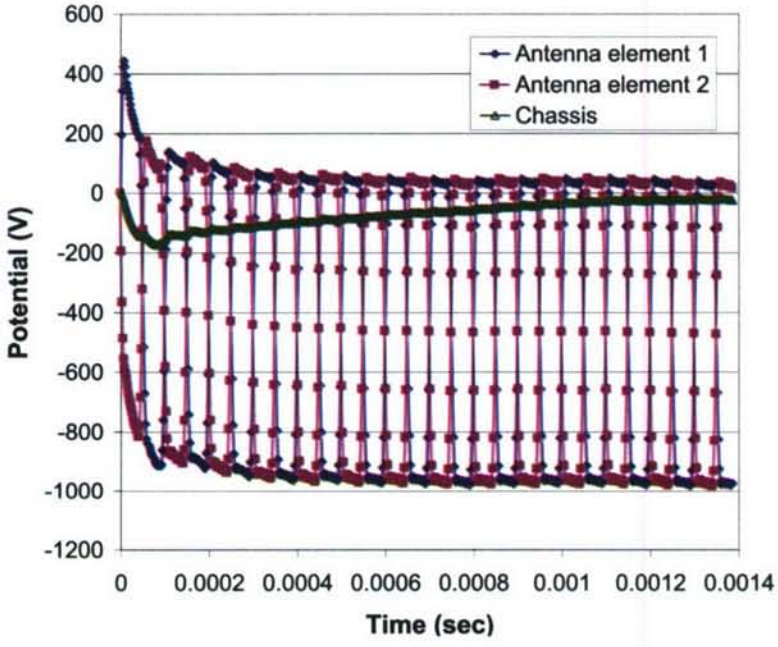

Figure 6. Time dependence of potentials for a 10^8 m^{-3} plasma at 10 kHz with no particle splitting (Case 1).

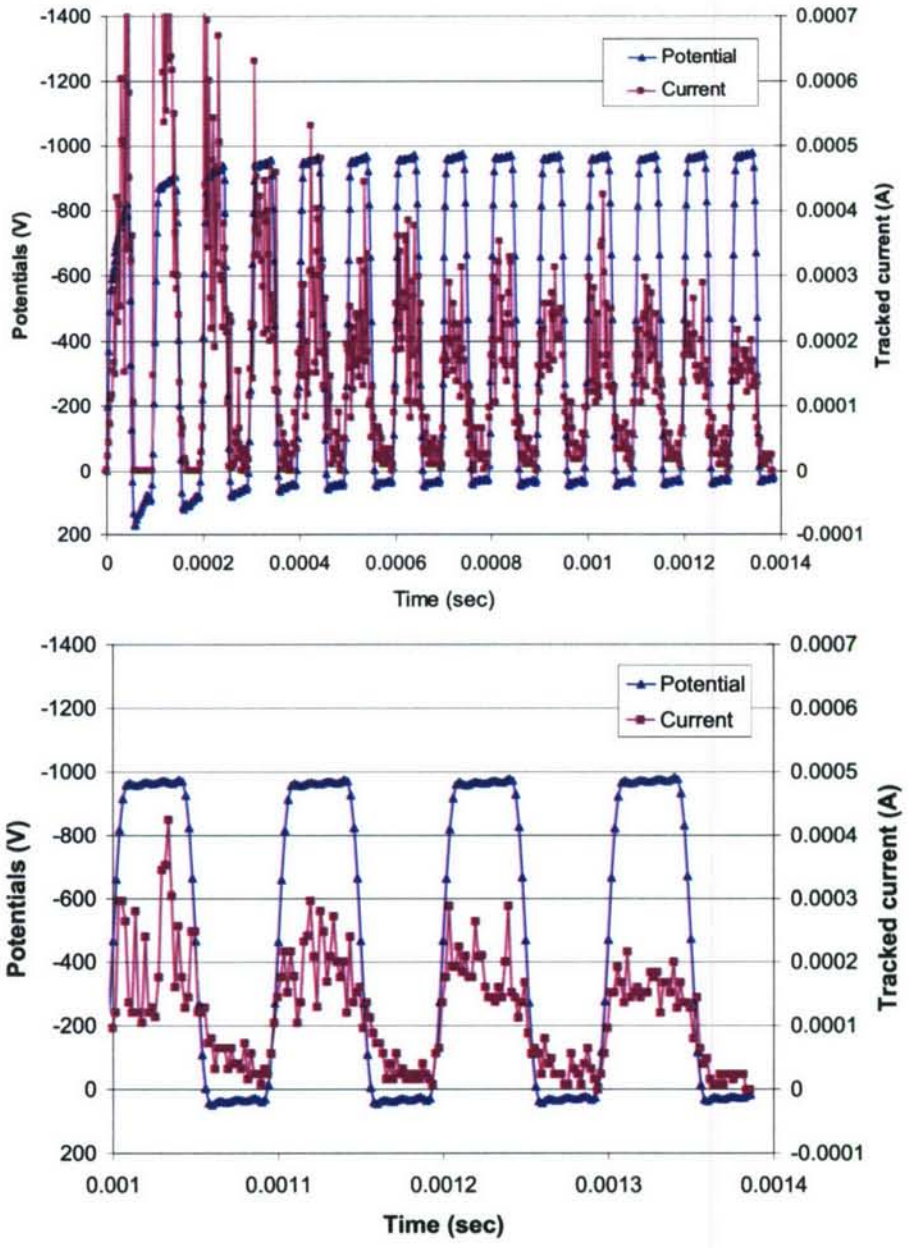

Figure 7. Potential and collected ion current of antenna element 2 for a 10^8 m^{-3} plasma at 10 kHz with no particle splitting (Case 1).

Case 2 has the same physical parameters as Case 1, but includes particle splitting, thus allowing both for smaller, more numerous particles and a representation of the thermal distribution. Figure 8 shows the potential distribution about the negative antenna element when fully biased at 2.11 ms, at the end of the simulation. At this low plasma density, the sheath nearly fills the grid and is more nearly spherical than cylindrical. The sheath also envelopes the positive antenna, providing a barrier to electrons, and thus allowing the system to float more positive than might be expected. (This barrier effect on electrons is not modeled in the present simulation.) The collected ion current, shown in Figure 9, is smoother, and by the end of the simulation has dropped to about 30 μA (8 μA m^{-2}), which is about four times orbit limited for a cylinder. This is reasonable because (1) the voltage is applied only half the time, and (2) additional current enters through the "end" of the sheath.

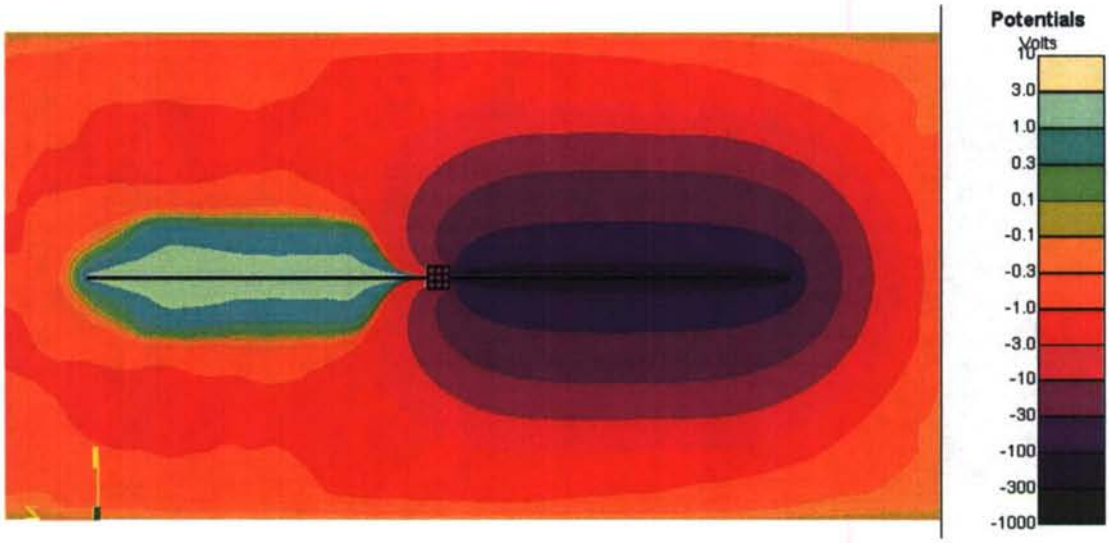

Figure 8. Potential structure in plane through center of spacecraft and antenna elements at 2.11 ms for a 10^8 m^{-3} plasma at 10 kHz (Case 2).

In both of the first two calculations, the plasma current to the negative antenna element responds almost immediately to the switch to negative potential, even though the applied frequency is well above the ion plasma frequency. This occurs because the applied electric fields are very high, and rapidly accelerate ions to speeds far in excess of their thermal velocity. However, the response to the positive switch is less sudden, and ions continue to be collected by the positive antenna element through nearly all its positive half-cycle. The fundamental frequency component of the current lags the applied voltage by a 10° phase shift, substantially less than the ninety degree shift expected in the linear regime.

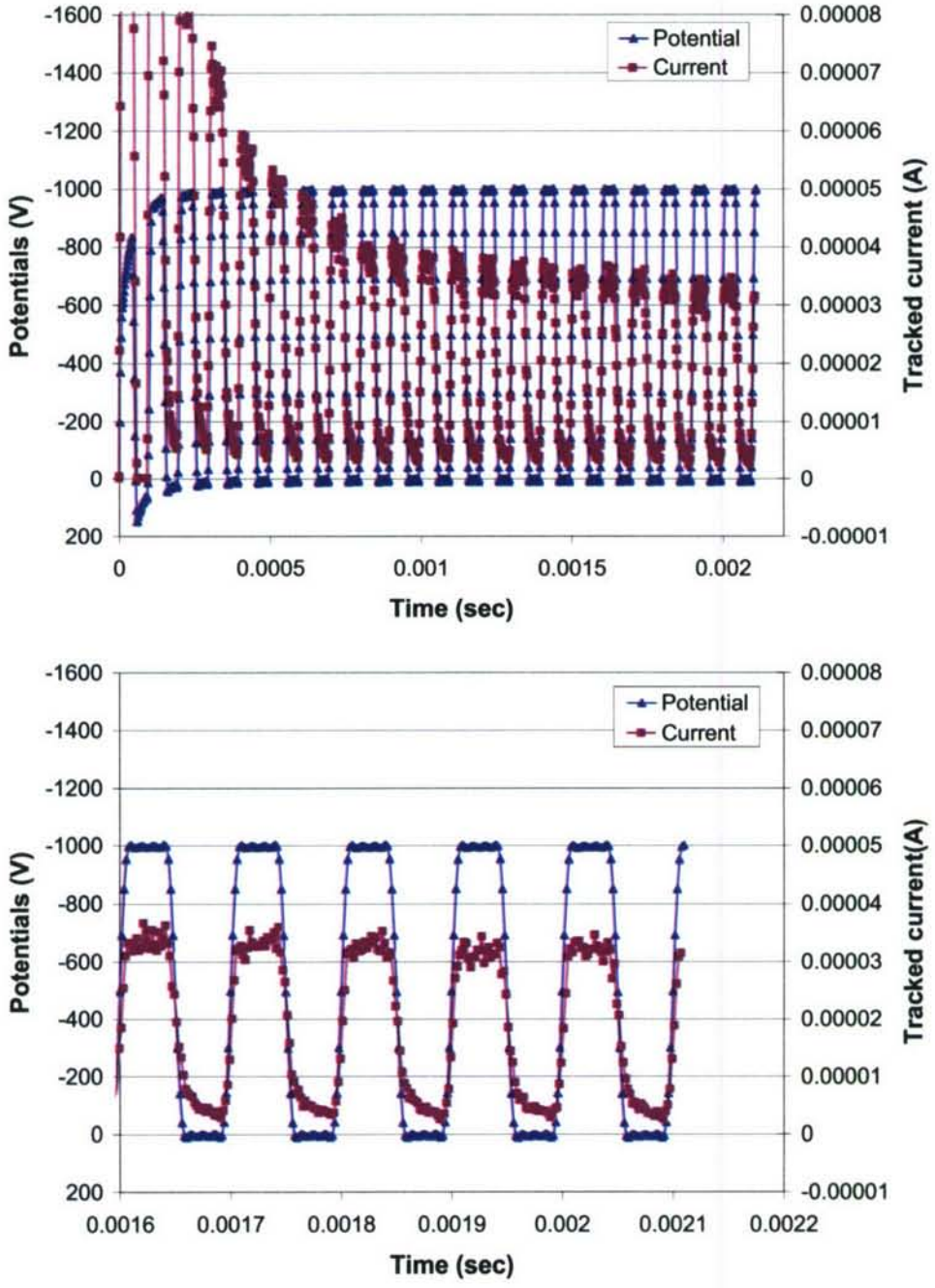

Figure 9. Potential and collected ion current of antenna element 2 for a 10^8 m^{-3} plasma at 10 kHz (Case 2).

Cases 3 and 4, at high and low frequency with respect to the ion plasma frequency, treat a plasma that is an order of magnitude more dense (10^9 m^{-3}) than the first two calculations, and thus has a considerably smaller sheath (Figure 10). The sheath is much more cylindrical in character than at lower density (Figure 8), but the spherelike end cap sheath remains substantial. (Noise in the background plasma shown in Figure 10 is at the 1 V level.) The antenna and spacecraft potentials (Figure 11) follow very much the same pattern as the more tenuous plasma (Figure 6), except that the positive potentials are better held in check by the higher electron current. Similar to the previous cases, a positive spike in potential is seen on switching. The current is 0.2 to 0.3 mA (80 μA m^{-2}), which is four times 20 μA m^{-2}, the orbit limited value for a cylinder in this plasma, and far less than

the spherical orbit limited value of 600 μA m^{-2}. The current variation over a cycle reaches repeating on the fifth cycle at 12 kHz and on the third cycle at 2 kHz. The current variation with time (Figure 12 and Figure 13) differs between the high and low frequency cases. Both show an initial rapid increase as ions within the sheath are collected. In the high frequency case (Figure 12) a further gradual increase occurs as ions near the sheath edge, which take longer to reach the antenna, are collected. The fundamental frequency component of the current lags the applied voltage by a 12° phase shift, more than that seen in the lower density case. In the low frequency case (Figure 13) all ions within the sheath are exhausted early in the pulse, and the collected current is limited to those ions eroded from the sheath edge during the pulse, resulting in decreasing current during most of the cycle. Consequently, the fundamental frequency component of the current leads the applied voltage by a phase shift of about 7°.

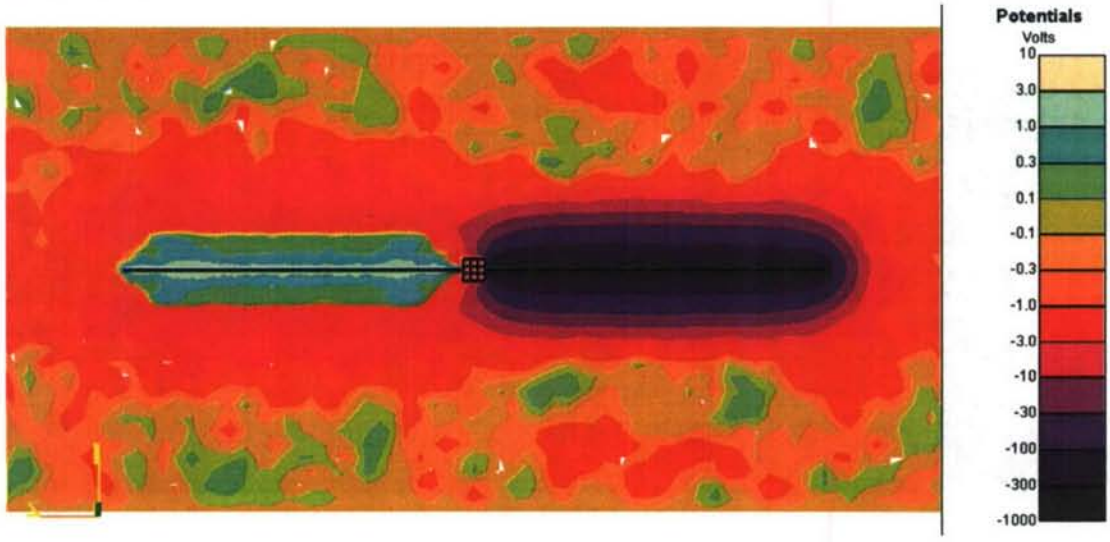

Figure 10. Potential structure in plane through center of spacecraft and antenna arms at 1.34 ms for the high density 10^9 m^{-3} plasma at 12 kHz (Case 3).

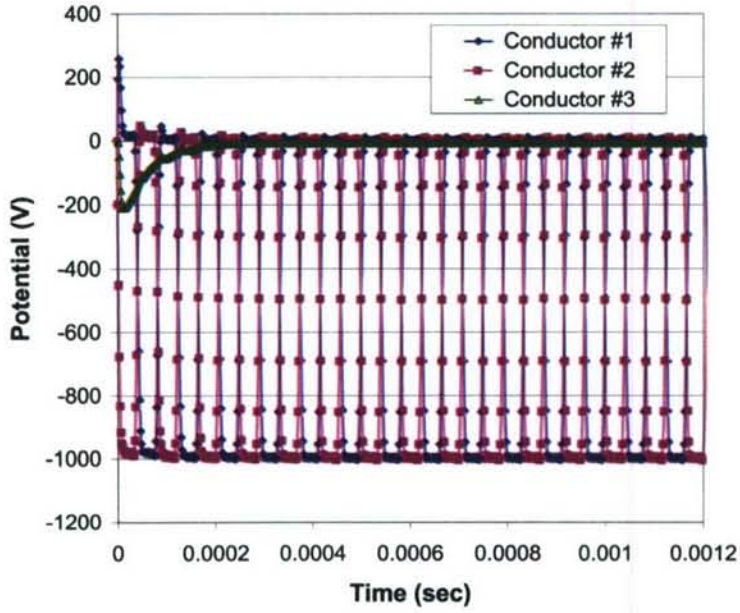

Figure 11. Time dependence of potentials for the high density 10^9 m^{-3} plasma at 12 kHz (Case 3).

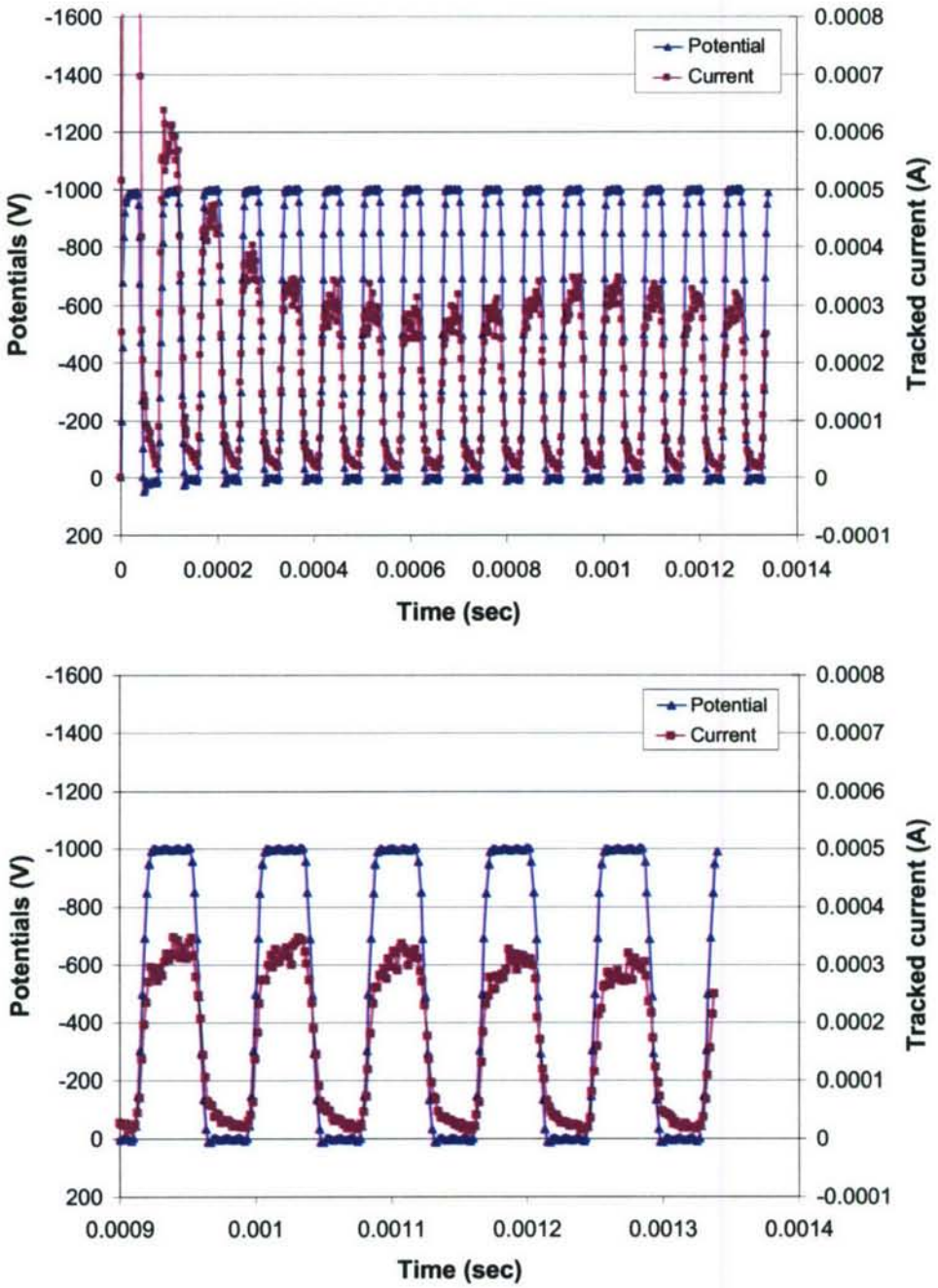

Figure 12. Potential and collected ion current of antenna element 2 for the high density 10^9 m^{-3} plasma at 12 kHz (Case 3). Note that the current lags the potential by a 12° phase shift.

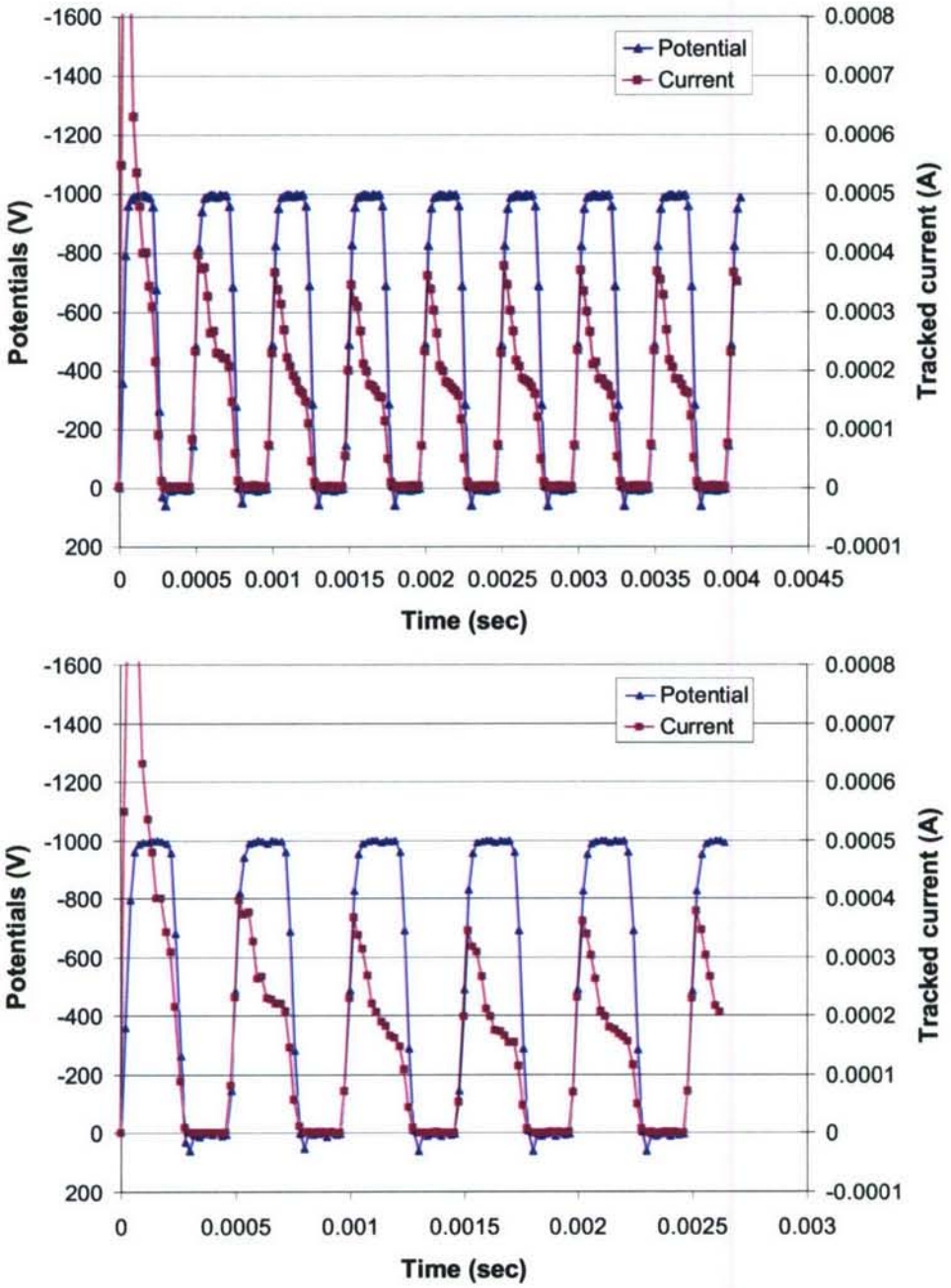

Figure 13. Potential and collected ion current of antenna element 2 for the high density 10^9 m^{-3} plasma at 2 kHz (Case 4). Note that the current leads the potential by a phase shift of about 7°.

Figure 14 illustrates the difference between the high and low frequency behavior. It shows the results of a one-dimensional calculation of a spherical antenna in a plasma of density 4×10^7 m^{-3} with applied sinusoidal potential of 5000V at 10 kHz (left) and 1 kHz (right). At high frequency the sheath (defined as the region from which electrons are excluded) extends far into the ambient plasma, and ions are collected only from the inner region of the sheath. The collected current can increase during the time the potential is applied as ions are collected from progressively farther out in the sheath at each cycle. By contrast, at low frequency the sheath region is nearly emptied at each cycle, so that the current must fall off as ions from the sheath edge region are difficult to collect.

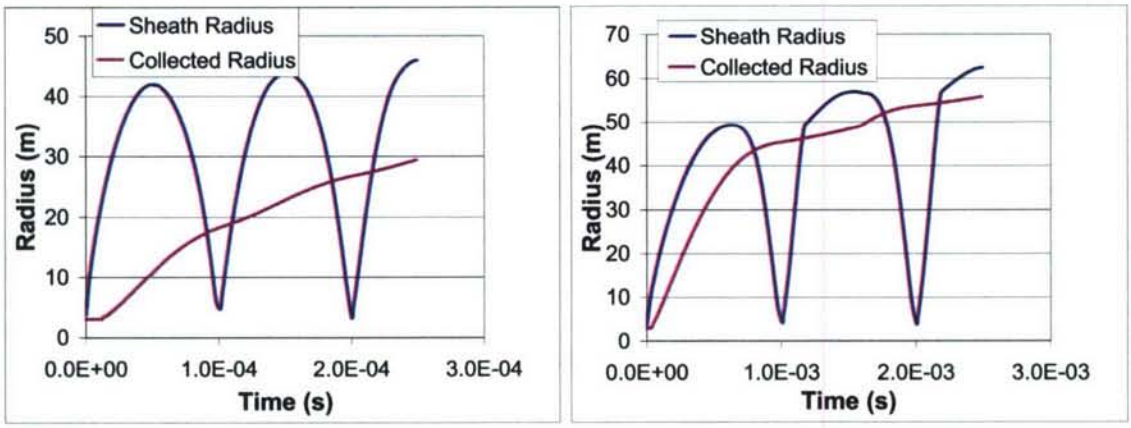

Figure 14. One dimensional spherical calculation of sheath radius and ion collection radius at high frequency (left) and low frequency (right).

4 - CONCLUSIONS

We have used *Nascap-2k* to study the plasma interactions of a high voltage near-square-wave VLF antenna in MEO plasma. The model consists of two 25 meter antenna elements biased ±1000 V at voltages above or below the ion plasma frequency. For these very high applied voltages, the plasma response is nonlinear, and the sheaths are more spherical than cylindrical, especially at the lower density. In modeling the system it is important to use particle splitting and injection techniques that replenish depleted plasma at boundaries, maintain appropriately sized macroparticles, and provide a reasonable representation of the plasma thermal distribution. When this is done, the incident current is in reasonable agreement with orbit-limited predictions.

When the excitation frequency is above the ion plasma frequency the plasma current to an antenna element increases sharply when the potential is applied, and falls off relatively slowly when it is removed, with incident ion current continuing substantially into the unbiased half-cycle. Below the ion plasma frequency the ion current peaks sharply when the potential is applied, falls off substantially during the half-cycle, and drops sharply to zero when the potential is removed. The difference can be understood in terms of the sheath being depleted of ions within every cycle at low frequency, but not at high frequency. The current lags the applied voltage for excitation frequencies above the ion plasma frequency by 10° at the low density and 12° at the high density, which is much less than the ninety degree shift expected in the linear regime. At low frequency (calculated for the high density only) the current leads the applied voltage by 7°

ACKNOWLEDGEMENTS

This paper was prepared with funding from the Air Force Research Laboratory.

REFERENCES

[1] Vampola, A. L., and G. A. Kuck, Induced precipitation of inner zone electrons, 1, Observations, *J Geophys Res, 83*, 2543, 1978.

[2] Imhof, W. L., E. E. Gaines, J. B. Reagan, Evidence for the resonance precipitation of energetic electrons from the slot region of the radiation belts, *J Geophys Res, 79*, 3141, 1974.

[3] Inan, U. S., H. C. Chang, R. A Helliwell, Electron precipitation zones around major ground-based VLF signal sources, *J Geophys Res, 89*, 2891, 1984.

[4] M.J. Mandell, D.L. Cooke, Nascap-2k as a PIC Code, *Proceedings of the 8th Spacecraft Charging Technology Conference*, Huntsville, AL, NASA/CP-2004-213091, 2003.

[5] M.J. Mandell, V.A. Davis, D.L. Cooke. A.T. Wheelock, C.J. Roth, Nascap-2k simulations of a VLF plasma antenna, *Proceedings of the 9th Spacecraft Charging Conference,* Tsukuba, Japan, Japan Aerospace Exploration Agency (JAXA), 2005.

[6] V.A. Davis, M.J. Mandell, D.L. Cooke, and C.L. Enloe, High-voltage interactions in plasma wakes: Simulation and flight measurements from the Charge Hazards and Wake Studies (CHAWS) experiment, *J Geophys Res, 104,* A6, p. 12445, 1999.